PCCP

ROYAL SOCIETY OF CHEMISTRY

PAPER

View Article Online
View Journal | View Issue

Cite this: *Phys. Chem. Chem. Phys.*, 2022, **24**, 12346

Pre-Dewar structure modulates protonated azaindole photodynamics†

Ritam Mansour, [a] Saikat Mukherjee, *[a] Max Pinheiro Jr., [a] Jennifer A. Noble, [b] Christophe Jouvet [b] and Mario Barbatti *[ac]

Received 4th March 2022,
Accepted 5th May 2022

DOI: 10.1039/d2cp01056a

rsc.li/pccp

Recent experimental work revealed that the lifetime of the S_3 state of protonated 7-azaindole is about ten times longer than that of protonated 6-azaindole. We simulated the nonradiative decay pathways of these molecules using trajectory surface hopping dynamics after photoexcitation into S_3 to elucidate the reason for this difference. Both isomers mainly follow a common ππ* relaxation pathway involving multiple state crossings while coming down from S_3 to S_1 in the subpicosecond time scale. However, the simulations reveal that the excited-state topographies are such that while the 6-isomer can easily access the region of nonadiabatic transitions, the internal conversion of the 7-isomer is delayed by a pre-Dewar bond formation with a boat conformation.

Introduction

Azaindoles are hetero-bicyclic aromatic organic compounds consisting of a pyrrole ring fused to a pyridine ring. Being structurally different from indoles only by one additional nitrogen in the 6-membered pyridine ring, the azaindole moiety exhibits interesting biochemical and pharmacological activities.[1,2] Scientists identified that methylated azaindole chromophores could serve as blue or even green fluorescence protein markers.[3] Among various structural isomers of *n*-azaindole, 7-azaindole derivatives (see Fig. 1 for the atom numbering) are excellent blue emitters for organic light-emitting diodes (OLEDs).[4]

Although one can find a handful of articles on 7-azaindole as an isolated monomer,[5–8] in dimeric forms[5,9–13] and in water and alcohol clusters,[11,14–20] only one recent article[21] to date shed light upon the photophysical relaxation mechanism of *n*-azaindole molecules by studying gas-phase excited-state dynamics. Experiments and theoretical calculations have also been devoted[16,18,22–24] to understanding the excited-state proton transfer and tautomerization mechanism of 7-azaindole with solvent molecules. On the other hand, very recently, Noble *et al.* performed[25] photo-fragmentation spectroscopy on the protonated *n*-azaindole isomers (*n*-AIH$^+$, n = 5, 6, 7) to explore the role of the *n*-nitrogen atom position in photodynamics. From the spectral line widths, they estimated the excited-state lifetimes ($\tau = \hbar/\delta E$) tabulated in Table 2 and proposed different decay mechanisms for the isomers. Surprisingly, the lifetime of the S_3 state in 7-AIH$^+$ is almost ten times larger than that of 6-AIH$^+$.

This paper aims to elucidate the disparity of excited-state lifetimes between 6- and 7-protonated azaindoles (6/7-AIH$^+$) using trajectory surface hopping (TSH) simulations.[26] TSH is a well-known and efficient way of simulating excited-state dynamics, where the nuclear wavepacket on an electronic state is represented by a swarm of independent trajectories classically propagating the nuclear degrees of freedom, and the negative energy gradient of the corresponding electronic state serves as the force acting on the nuclei. A stochastic process dictates whether the trajectory will propagate on the current electronic state or hop to another one at each time step. Such a state switch mainly occurs in regions of strong nonadiabatic coupling. Among various strategies to compute hopping probabilities, we adopted the decoherence-corrected[27] fewest switches surface hopping[28] (DC-FSSH) algorithm, probably the most common and extensively reviewed in literature.[29] Despite a few shortcomings, an ensemble of independent DC-FSSH trajectories is expected to provide a reasonable semi-quantitative description of a photodynamic process in the sub-picosecond timescale.

Computational methods

The ground state geometry optimization followed by normal-mode analysis for both protonated species, 6- and 7-AIH$^+$, was performed with Møller–Plesset perturbation theory to the

[a] *Aix Marseille University, CNRS, ICR, Marseille, France.*
E-mail: saikat.mukherjee@univ-amu.fr
[b] *Aix-Marseille University, CNRS, PIIM, Marseille, France*
[c] *Institut Universitaire de France, 75231 Paris, France.*
E-mail: mario.barbatti@univ-amu.fr

† Electronic supplementary information (ESI) available. See DOI: https://doi.org/10.1039/d2cp01056a

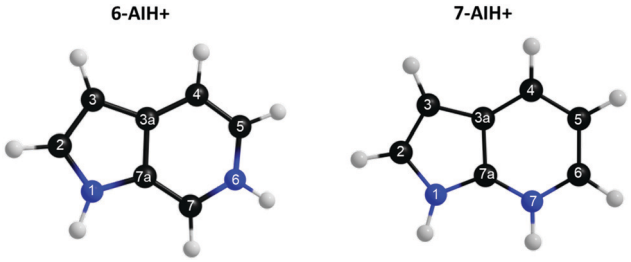

Fig. 1 Structure and atom labeling for 6- and 7-protonated azaindole molecules.

Table 1 Experimental spectral width and derived lifetimes of *n*-AIH$^+$ isomers from ref. 25

		5-AIH$^+$	6-AIH$^+$	7-AIH$^+$
S_1	δE (cm^{-1})	<10	<10	<10
	τ (fs)	$>\sim530$	$>\sim530$	$>\sim530$
S_2	δE (cm^{-1})	280	115	Not visible
	τ (fs)	~20	~50	
S_3	δE (cm^{-1})	Not probed	230	23
	τ (fs)		~25	~230

second-order (MP2) with the aug-cc-pVDZ basis set.[30,31] The excited states were calculated with the resolution-of-identity algebraic diagrammatic construction to the second-order (RI-ADC(2))[32,33] with the same basis set. The electronic structure calculations were carried out with Turbomole (version 7.3).[34,35] The geometries of the intersections between the excited states S_3/S_2 and S_2/S_1 were located using the penalty function method implemented in the Conical Intersection Optimizer (CIOpt) program[36,37] and adapted by us to work with Turbomole.

Five hundred initial conditions were sampled from a harmonic oscillator Wigner distribution[38,39] using the ground-state geometry and normal modes. The absorption spectra into eight excited states for both species were simulated[40] for these initial conditions (see Fig. S1 in the ESI†). For 6-AIH$^+$, we have chosen 60 initial conditions in the energy window 5.5 ± 0.2 eV to start trajectories in the S_3 state (ESI,† SI-1). For 7-AIH$^+$, we selected 84 initial conditions in the same energy window, to start trajectories also in S_3.

The DC-FSSH dynamics were employed to simulate the nonadiabatic relaxation process for both molecules. We have included four singlet electronic states (including the ground state, S_0) calculated at ADC(2)/aug-cc-pVDZ level of theory in the direct dynamics simulation. The trajectories were launched from the bright S_3 state and propagated up to 1000 fs for both molecules. The classical equations of motion were integrated with a 0.5 fs time step using the velocity Verlet algorithm, whereas the locally-approximated time-dependent Schrödinger equations were integrated with 0.025 fs using interpolated electronic quantities between classical steps. Energy-based decoherence corrections were applied with the simplified decay of mixing approach with the parameter α set to 0.1 a.u. Time-derivative couplings between excited states were calculated with the Hammes–Schiffer and Tully approach[41] using the determinant derivative approach.[42] After a successful hop, the energy was balanced by rescaling the nuclear velocity in the direction of the momentum vector. In the case of frustrated hopping, the momentum direction was not changed. DC-FSSH was employed to evaluate hoppings between excited states only. Due to the limitation of ADC(2) to describe the multireference character of the S_1/S_0 crossing, whenever the energy gap between these states dropped to below 0.15 eV, the trajectory propagation was ended, and we assumed the molecule returned to the ground state.

The initial conditions sampling, absorption spectra calculations, and DC-FSSH simulations were carried out with Newton-X (version 2.2 build 12)[43] interfaced with Turbomole. The dataset of all the trajectories[44] and processed data[45] for each azaindole isomer are available to download.

Results

Excited-state topography

We optimized the geometries of the ground- (S_0) and excited-state (S_1 to S_3) minima and the S_3/S_2 and S_2/S_1 intersections of 6- and 7-AIH$^+$. The results are shown in Table 2 and Fig. 2. The excitation character of the electronic states and molecular orbitals associated with the corresponding excitation are presented in the SI-2 and SI-3 (ESI†). Cartesian coordinates of all structures are also given in the ESI.†

At the ground state minimum of both the molecules, S_3 is a bright state with $\pi\pi^*$ character. At the S_3 minimum, the energy gap to S_2 is 0.58 eV for 6-AIH$^+$ and 0.71 eV for 7-AIH$^+$. After populating S_2, both molecules should relax toward the S_2 minimum. There, the energy gap to S_1 is 0.36 eV for 6-AIH$^+$ and 0.24 eV for 7-AIH$^+$. At the S_1 minimum, the energy gaps to S_0 are 3.32 and 2.75 eV for 6- and 7-AIH$^+$, respectively. The S_3/S_2

Table 2 Excitation energies at the minima of the S_0 to S_3 states computed with ADC(2)/aug-cc-pVDZ. All values are relative to the ground state minimum. Oscillator strengths are given in the brackets. The adiabatic energies observed in the experiment[25] are shown within the parenthesis. X indicates the state intersection. All minima have $\pi\pi^*$ character

	6-AIH$^+$				7-AIH$^+$			
Geom.	ΔE_0/eV	ΔE_1/eV [f_{10}]	ΔE_2/eV [f_{20}]	ΔE_3/eV [f_{30}]	ΔE_0/eV	ΔE_1/eV [f_{10}]	ΔE_2/eV [f_{20}]	ΔE_3/eV [f_{30}]
S_0 min	0.00	3.95 [0.12]	5.01 [0.05]	5.77 [0.48]	0.00	3.97 [0.03]	4.55 [0.17]	5.87 [0.54]
S_1 min	0.34	3.66 [0.11] (3.61)	5.17 [0.02]	5.83 [0.52]	0.70	3.45 [0.03] (3.50)	4.91 [0.12]	5.97 [0.46]
S_2 min	0.86	4.48 [0.11]	4.84 [0.11] (4.67)	6.30 [0.15]	0.41	4.06 [0.03]	4.30 [0.20] (4.41)	6.14 [0.24]
S_3 min	0.21	3.92 [0.1]	4.97 [0.02]	5.55 [0.44] (5.43)	0.52	3.97 [0.02]	4.76 [0.04]	5.47 [0.53] (5.47)
S_3/S_2 X	2.59	5.99 [0.03]	6.83 [0.04]	6.85 [0.27]	2.34	4.99 [0.01]	5.99 [0.02]	6.01 [0.20]
S_2/S_1 X	1.22	4.84 [0.04]	4.86 [0.24]	6.56 [0.02]	0.53	4.31 [0.03]	4.32 [0.21]	6.28 [0.15]

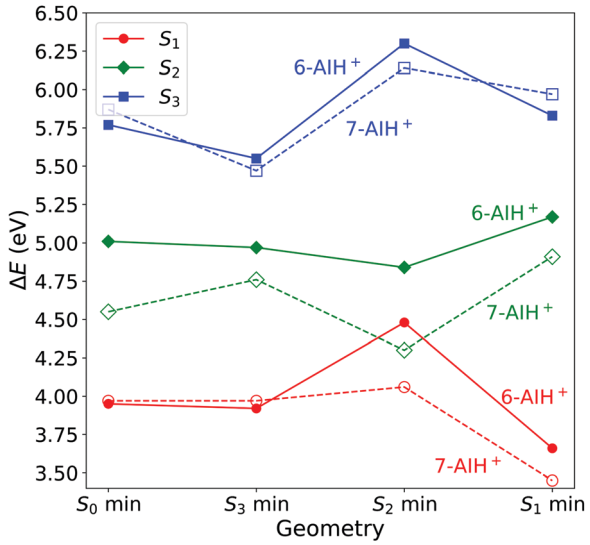

Fig. 2 Excitation energies at the minima of the S_0 to S_3 states computed with ADC(2)/aug-cc-pVDZ. All values are relative to the ground state minimum.

intersection is 1.28 eV higher than the S_3 minimum in 6-AIH$^+$ but only 0.5 eV higher in 7-AIH$^+$. In S_2, the S_2/S_1 intersections lie very close to their corresponding S_2 minimum for both isomers.

These topographic features do not deliver any indication of why the S_3 lifetime is much shorter in 6-AIH$^+$ than in 7-AIH$^+$.

Dynamics

Next, we will describe the outcomes from the DC-FSSH dynamics. Fig. 3 depicts the evolution of the adiabatic population for both species. We fitted the S_3 population of 6-AIH$^+$ with the exponential decay function

$$f(t) = e^{-t/\tau} \quad (1)$$

For 7-AIH$^+$, eqn (1) did not fit the population well, and we needed a second exponential component,

$$f(t) = (1 - A)e^{-t/\tau'} + Ae^{-t/\tau}. \quad (2)$$

Later we discuss that this component is due to dissociative trajectories occurring only for 7-AIH$^+$. The results of the fitting are summarized in Table 3. The margins of error were computed for a 95% confidence interval.

After excitation into the S_3 state, both molecules undergo internal conversion to S_2 and, then, to S_1 in the sub-ps time scale. In 6-AIH$^+$, the S_3 state deactivates within 156 ± 40 fs, while this process takes longer in 7-AIH$^+$, 278 ± 36 fs. 7-AIH$^+$ also shows partial internal conversion to S_0 within this time (Fig. 3).

The energy-gap distributions at the hopping time are shown in Fig. 4 for $S_3 \rightarrow S_2$ and $S_2 \rightarrow S_1$ transitions. The hoppings from S_3 to S_2 (top) are distributed around a relatively large energy gap for both molecules. The distribution follows approximately a Gaussian shape centered around a mean value of 0.47 eV for both 6- and 7-AIH$^+$, respectively, while the standard deviation is 0.13 eV for 6-AIH$^+$ and 0.22 eV for

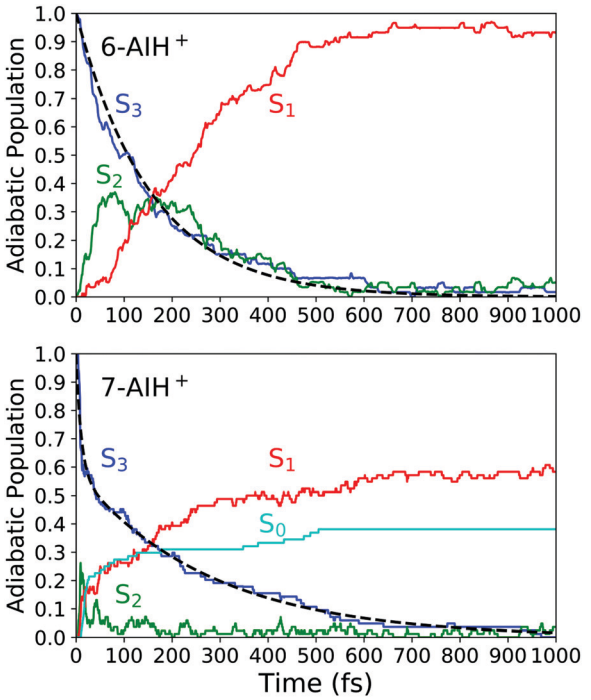

Fig. 3 Adiabatic population evolution calculated with ADC(2)/aug-cc-pVDZ for 6-AIH$^+$ (top) and 7-AIH$^+$ (bottom). The dashed line indicates the S_3 population fitting.

Table 3 Fitted parameters of the S_3 population curves of 6- and 7-AIH$^+$ for simulations at ADC(2)/aug-cc-pVDZ. Experimental lifetimes from ref. 46 are shown in parenthesis. The margins of error are estimated for a 95% confidence interval

	A	τ' (fs)	τ (fs)
6-AIH$^+$	—	—	156 ± 40 (~25)
7-AIH$^+$	0.58	11	278 ± 36 (~230)

7-isomer. These gap distributions are due to the large energies of the S_3/S_2 intersections compared to the S_3 minimum (see Table 2). On the other hand, the energy gap histogram for $S_2 \rightarrow S_1$ hoppings resembles an exponential distribution (Fig. 4-bottom). For 6-AIH$^+$, the mean value and standard deviations are 0.23 and 0.20 eV, while for 7-AIH$^+$, they are 0.17 and 0.14 eV.

In the case of the $S_3 \rightarrow S_2$ hoppings, the large energy gap distribution may seem incompatible with the short S_3 state lifetimes. Nevertheless, although the S_3/S_2 intersection is not reached during dynamics, the S_3/S_2 energy gap remains relatively small. While 6-AIH$^+$ is on S_3, the mean S_3/S_2 gap is 0.60 eV with a 0.13 eV standard deviation. For 7-AIH+, the mean value is 0.76 eV, and the standard deviation is 0.19 eV. This energetic proximity between the S_3 and S_2 states during dynamics in S_3 increases the number of timesteps where potentially a hopping can occur, compensating for the small probabilities. We discuss this aspect in detail in Section Hoppings at large energy gaps.

We also analyzed the state character at the hopping time by checking the density difference between the current and

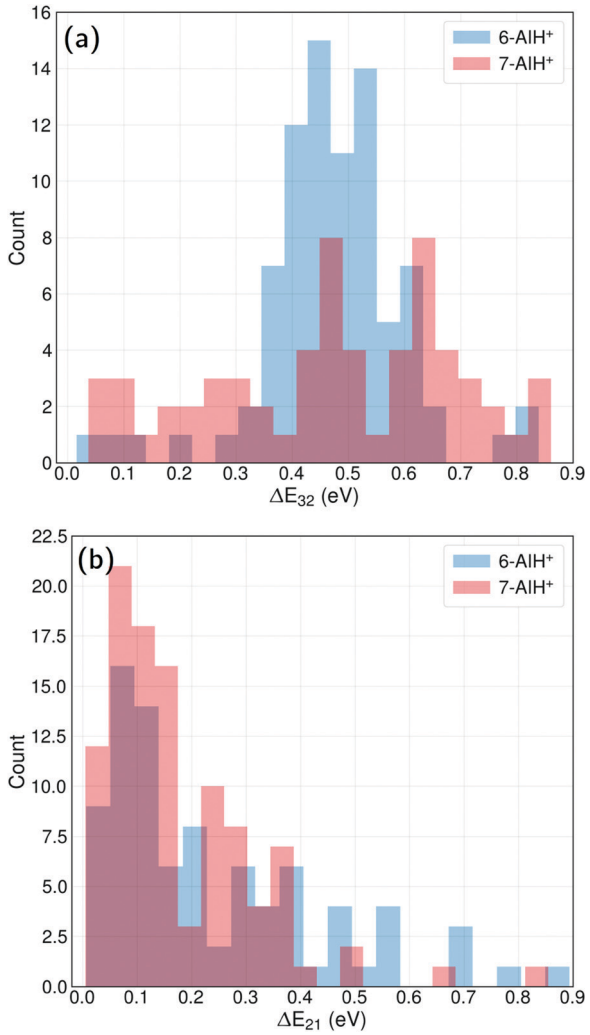

Fig. 4 Energy gap distributions between (a) $S_3 \rightarrow S_2$ states and (b) $S_2 \rightarrow S_1$ states considering only geometries at the hopping points for both the molecules. The 7-AIH$^+$ dissociating trajectories (38%) are excluded.

ground states (SI-4, ESI†). The result of this analysis is shown in Table 4.

Discussion

Topography and dynamics

In the ground state, 6-AIH$^+$ is perfectly planar, and it retains the planarity in the S_1 and S_3 state minima too. Nevertheless, its S_2 state minimum is puckered with a boat distortion of the 6-membered ring, involving atoms C5 and C7a. Its Cremer–Pople Q parameter[47] is 0.24 Å. (The Q parameter indicates the puckering intensity, with $Q = 0$ being a planar ring.) In turn, 7-AIH$^+$ is planar in the ground state and puckered in the S_3 excited state, also with a C5–C7a boat conformation (Q = 0.18 Å). This out-of-plane minimum is in good agreement with the experiment, which exhibits a low-frequency vibrational progression in S_3 assigned to out-of-plane modes.[25] The rings in the S_1 and S_2 minima are planar with the H atom attached with the 6-membered ring N atom is marginally out of the plane.

The 6-AIH$^+$ S_2 minimum and 7-AIH$^+$ S_3 minimum have a boat conformation involving atoms C5 and C7a. Fig. 5 shows that these two atoms receive π-density and that the π* molecular orbital has an in-phase alignment across the ring. These features indicate that a pre-Dewar structure forms between C5 and C7a across the ring. Nevertheless, the puckering degree is too small to characterize it as a Dewar bond. The density differences in Fig. 5 reveal that these two atoms have more π density in 6- than in 7-AIH$^+$, explaining why the puckered ππ* minimum is more stable in the former. This figure also shows that while the nitrogen atom in position 6 is an electron donor, it is an electron acceptor in position 7.

These potential energy surface (PES) topographies give rise to the following dynamics. After 6-AIH$^+$ is vertically lifted to the S_3 state, it relaxes to the planar S_3 minimum within only 20 fs (Fig. 6, left). This fast relaxation is due to the geometric proximity between the S_3 and S_0 minima, which are only 0.03 Å apart, as measured by the root-mean-square deviation

Table 4 Fraction of $S_3 \rightarrow S_2$ and $S_2 \rightarrow S_1$ hoppings occurring only between ππ* states and involving at least one πσ* state. For 7-AIH$^+$, dissociative trajectories are not included

		6-AIH$^+$ (%)	7-AIH$^+$ (%)
$S_3 \rightarrow S_2$	Only ππ*	97	75
	At least one πσ*	3	25
$S_2 \rightarrow S_1$	Only ππ*	98	98
	At least one πσ*	2	2

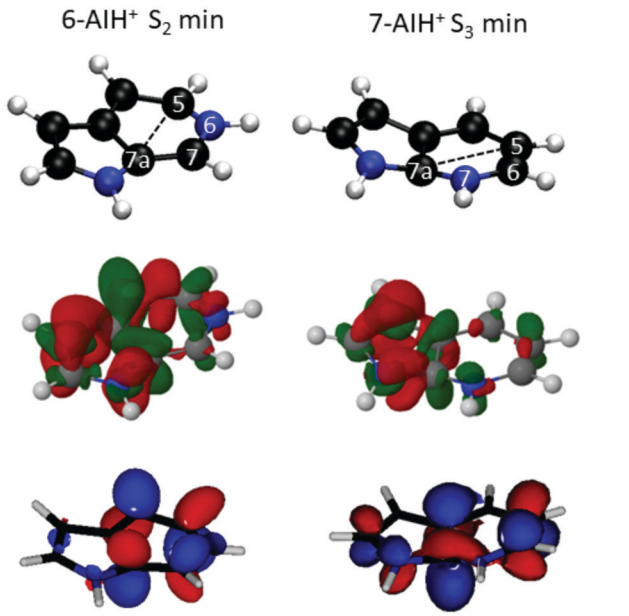

Fig. 5 The top panel highlights the C5 and C7a atoms involved in the boat conformation leading to pre-Dewar structures. The middle panel shows the density difference between the S_2 and S_0 states at the S_2 minimum of 6-AIH$^+$(Left) and the same between the S_3 and S_0 states at the S_3 minimum of 7-AIH$^+$ (Right). The electron is promoted from the red to green regions. The bottom panel displays the π* molecular orbital for S_2 minimum of 6-AIH$^+$(Left) and S_3 minimum of 7-AIH$^+$ (Right).

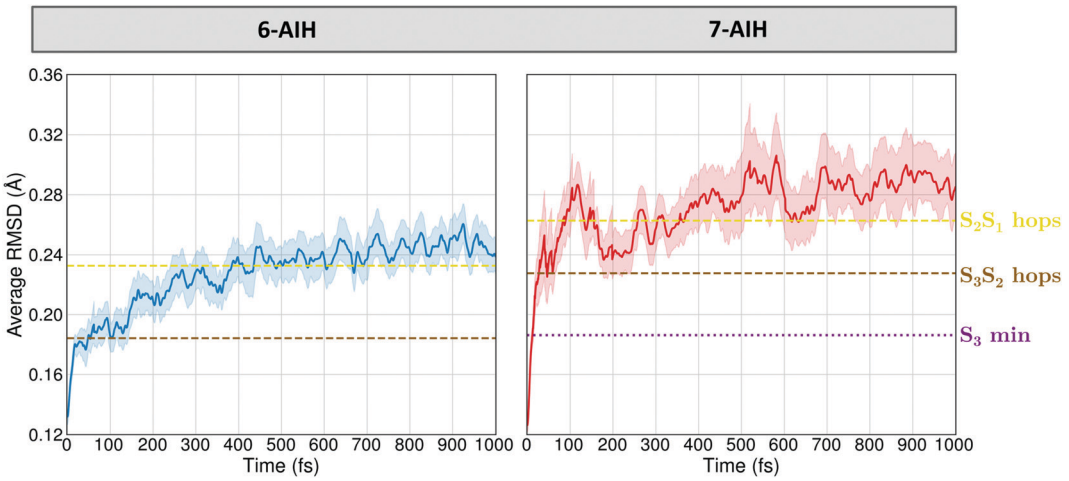

Fig. 6 Time evolution of the average RMSD between the molecular geometries obtained during the dynamics simulation and the ground state reference configuration.

(RMSD) between them. Then, it undergoes $S_3 \rightarrow S_2$ hopping within 156 fs. In S_2, it relaxes to the puckered S_2 minimum. The population accumulates there, growing up to 30% before it transfers to the S_1 state within 300 fs. In the case of 7-AIH$^+$, it relaxes to the S_3 minimum within about 40 fs (Fig. 6, right). This minimum is located 0.19 Å from the S_0 minimum. After that, the molecule takes longer to hop to S_2, yielding an S_3 lifetime of 268 fs. The population does not accumulate in S_2, and it is immediately transferred to S_1.

In both molecules, the $S_3 \rightarrow S_2$ hopping events take place at significant energy gaps, about $\sim$0.4 eV (Fig. 4-top) due to the high energy of the S_3/S_2 intersection. On the other hand, the $S_2 \rightarrow S_1$ hopping energy gap peaks at $\sim$0.1 eV (Fig. 4-bottom) thanks to the more energetically favourable S_2/S_1 intersection being isoenergetic with the S_2 minimum.

The $S_3 \rightarrow S_2$ hopping geometries are characterized with the Cremer–Pople parameters[47] Q, θ, and ϕ. The parameters θ and ϕ describe the type of puckering the 6-membered ring undergoes. Q, as mentioned, indicates the puckering intensity. Fig. 7 shows that the $S_3 \rightarrow S_2$ hoppings happen in the entire θ–ϕ space. Later we discuss how this distribution helps understand the S_3 lifetimes of 6- and 7-AIH$^+$.

7-AIH$^+$ shows an additional feature not present in the dynamics of 6-AIH$^+$. A fraction of 38% of 7-AIH$^+$ trajectories quickly dissociates (11 fs), losing the hydrogen attached to the 5-membered ring. During this dissociation, the molecule returns to the ground state, forming the S_0 population we can see in the bottom panel of Fig. 3.

S_3 lifetimes

Before comparing the S_3 lifetimes of the two molecules, we should consider the short time constant (11 fs; Table 3) we observed in 7-AIH$^+$ simulations. As explained, this time constant is associated with dissociative trajectories, which must correspond to excitation to an unbound state. However, the experiments were done with a sharp excitation into the bound

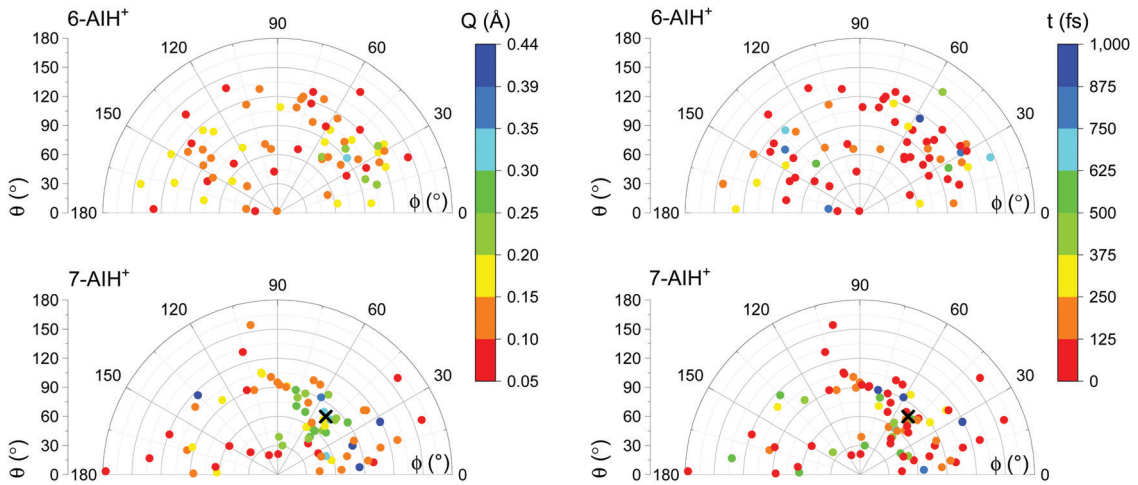

Fig. 7 Cremer–Pople parameters at the $S_3 \rightarrow S_2$ hopping points for 6-AIH$^+$ (top) and 7-AIH$^+$ (bottom). The colour indicates the Q value in the graphs on the left and the hopping time on the right. A cross marks the puckered S_3 minimum of 7-AIH$^+$. The planar S_3 minimum is not shown.

0–0 S_3 band origin.[25] On the contrary, the initial conditions for dynamics were created with energy exceeding the 0–0 band due to software limitations (see SI-1, ESI†). Thus, when comparing theory to the experiments, we should only consider the long S_3 lifetime predicted for 7-AIH$^+$.

If we bear these considerations in mind, the dynamics simulations predict a shorter S_3 lifetime for 6-AIH$^+$ (156 fs) than for 7-AIH$^+$ (278 fs). The value for 7-AIH$^+$ agrees well with the experimental measurement ($\sim$230 fs). The one for 6-AIH$^+$, however, is considerably longer than the experimental S_3 lifetime, $\sim$25 fs. While comparing the simulated lifetimes with the experimental ones, the following points are need to be considered. The accuracy of such small lifetimes is limited by the accuracy of the quantum-chemical level, and small errors in the PESs cause disproportionally large relative errors in the lifetime description. Moreover, the experimental lifetimes are indirectly obtained from linewidths through the time-energy uncertainty relation. Thus, they are themselves subject to uncertainties in the linewidth definition, estimation and even which uncertainty-relation to adopt.[48]

The different S_3 lifetimes of the two isomers mainly reflect the time for moving from the S_3 minimum to the region of $S_3 \rightarrow S_2$ hopping. As shown in Fig. 8, the $S_3 \rightarrow S_2$ hopping geometries are farther away from the S_3 minimum for 7-AIH$^+$ than for 6-AIH$^+$. This happens because the planar S_3 minimum of 6-AIH$^+$ provides easy access to the entire puckering conformational space, while the puckered pre-Dewar S_3 minimum of 7-AIH$^+$ does not. The Cremer–Pople puckering analysis of all points in S_3 during the dynamics shows that the trajectories span the entire puckering space uniformly and with a small puckering degree in 6-AIH$^+$, while they tend to cluster around the C5–C7a boat conformation with a more significant puckering degree in 7-AIH$^+$ (ESI,† SI-7). These distributions are what we would expect for a motion around the S_3 minimum of these two molecules, which is planar for 6-AIH$^+$ and puckered (C5–C7a boat with Q = 0.18 Å, θ = 78°, and ϕ = 50°) for 7-AIH$^+$.

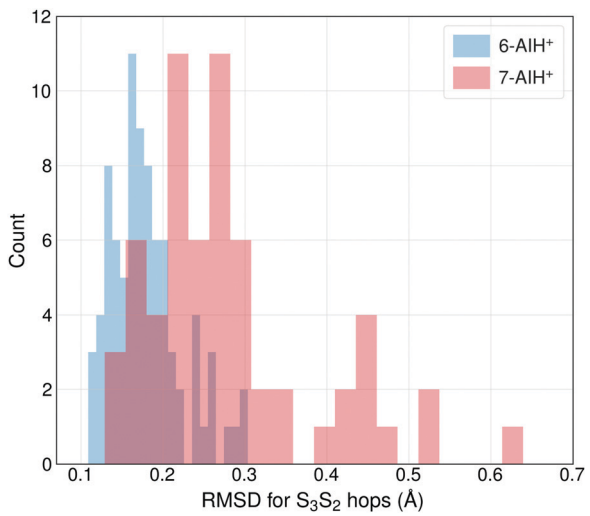

Fig. 8 The distribution of the RMSDs for $S_3 \rightarrow S_2$ hopping geometries, taking the S_3 minimum geometry as the reference.

As we have discussed, no specific coordinate causes the $S_3 \rightarrow S_2$ hopping. They occur during the motion around the S_3 minimum due to small but sizable probabilities resulting from the S_2–S_3 energetic proximity (as mentioned in Section Dynamics, the mean S_3/S_2 energy gap during S_3 dynamics is 0.6 eV for 6-AIH$^+$ and 0.8 eV for 7-AIH$^+$). Nevertheless, we observed an insightful correlation between the $S_3 \rightarrow S_2$ hopping and the puckering in the 7-AIH$^+$ case. To reach the hopping region, 7-AIH$^+$ (bottom-left graph in Fig. 7), which is clustered at low-puckered C5–C7a boat structures during the S_3 dynamics, either needs to increase its puckering degree in this boat region or change the puckering conformation. Either way, these processes take time, delaying the internal conversion. For 6-AIH$^+$ (top-left graph in Fig. 7), the hoppings tend to happen with slightly puckered geometries. (Note the dominance of red and orange points.) On the other hand, for 7-AIH$^+$ (bottom-left graph in Fig. 7), there are many hoppings at strongly puckered geometries (green and blue points).

The internal conversion delaying effect of the pre-Dewar character is also present in the $S_2 \rightarrow S_1$ transition, although less pronounced. In 6-AIH$^+$, where the S_2 minimum has the boat conformation, the population accumulates in S_2 before transferring to S_1 (Fig. 3-top). The hopping to S_1 happens, on average, 140 fs after the hopping to S_2. On the other hand, in 7-AIH$^+$, which has a planar S_2 minimum, the population is immediately transferred to S_1, without accumulating in S_2 (Fig. 3-bottom). The hopping to S_1 happens on average only 38 fs after the hopping to S_2. This very fast S_2 deactivation should give rise to wide experimental bands when exciting the molecule in this state, helping to explain why the experiments are unable to clearly distinguish S_2, as it was hidden in the higher energy part of S_1.

The hypothesis that Dewar structures play a role in the S_3 lifetime of 6- and 7-AIH$^+$ had already been raised in ref. 25. However, in that paper, the discussion focused on Dewar bonds between atoms 4 and 7, while here, we see them between atoms 5 and 7a.

State character

As experimentally predicted, the dynamics of 6-AIH$^+$ is entirely dominated by ππ* states. Both crossing states have ππ* character in 97% of the $S_3 \rightarrow S_2$ hopping events (Table 4). Nevertheless, in the case of 7-AIH$^+$, πσ* states play a minor but relevant role. During the $S_3 \rightarrow S_2$ internal conversion, the trajectories contributing to the long time constant (278 fs) are split into 75% with ππ*/ππ* crossings and 25% with hoppings involving at least one πσ* state. The occurrence of πσ* states was always associated with elongation to the NH bond distance in the 5-membered ring.

For both molecules (and considering only the non-dissociative trajectories of 7-AIH$^+$), the $S_2 \rightarrow S_1$ hopping is dominated by ππ*/ππ* crossings (98%). Naturally, the 7-AIH$^+$ dissociative trajectories deactivate through hoppings involving πσ* states.

Hoppings at large energy gaps

The usual interpretation of surface hopping is that the hopping event happens at the state crossing. However, actual hoppings

happen at small, non-null energy gaps, usually following (but not always) an exponential probability distribution. For example, in the case of ethylene's surface hopping dynamics reported in ref. 49, the $S_1 \rightarrow S_0$ energy gap at the hopping time is exponentially distributed with a 0.5 eV mean value. In fulvene,[50] the $S_1 \rightarrow S_0$ energy gap at the hopping time is exponentially distributed with a 0.3 eV mean value.

In AIH^+, the energy gaps at the $S_2 \rightarrow S_1$ hoppings also follow an exponential distribution, with a mean value of 0.23 eV for the 6-isomer and 0.14 eV for the 7-isomer. Nevertheless, the $S_3 \rightarrow S_2$ hoppings do not follow an exponential distribution because the S_3/S_2 state intersection is not energetically accessible. The distribution peaks at a non-zero value for both molecules, implying that it should tend to a Gaussian probability function if the statistics are improved. As reported in Section Dynamics, the mean value is 0.47 eV in both cases.

At first sight, such a large mean energy gap may seem incompatible with the short S_3-state lifetimes for 6- and 7-AIH^+: 156 and 278 fs, respectively. However, the hopping probability values are not unexpectedly large. For 6-AIH^+ in the S_3 state, the hopping probabilities to S_2 (considering only non-null values) are exponentially distributed with a mean value of 3×10^{-4} per sub-timestep (0.025 fs). For 7-AIH^+, this value is 2×10^{-4} per sub-timestep.

The lifetime is short for such small probabilities because of the energetic proximity between S_3 and S_2. (Recall the mean energy gap during S_3 dynamics is 0.6 and 0.8 eV for 6- and 7-AIH^+, respectively.) These relatively small gaps increase the number of time steps where potentially a hopping can occur. For instance, 12% of the sub-timesteps of 7-AIH^+ have a hopping probability bigger than 10^{-5}. This situation contrasts with the typical S_0/S_1 transition through state intersections (like in ethylene[49] or fulvene[50]), where internal conversion can occur only after the gap reduces enough to yield appreciable hopping probabilities.

Basis set effects

All results we reported in the previous sections were computed with the aug-cc-pVDZ basis set. Nevertheless, we have also used the cc-pVDZ basis set for fast, exploratory calculations. It may interest the readers to know the differences between these two sets of results. The main results are summarized in SI-5 (ESI†).

The static excited-state topography obtained by using the cc-pVDZ basis set (SI-5, ESI† and Table 1) remains approximately the same as that obtained by using the augmented one. The results of dynamics are also qualitatively the same. However, the population profiles differ quantitatively when comparing the results of aug-cc-pVDZ (Fig. 3) and cc-pVDZ (SI-5, ESI†). With the smaller basis set, the S_3 lifetime of 6-AIH^+ decreases to 136 fs, whereas for 7-isomer it increases to 361 fs. Also, there are no dissociative trajectories for either isomer with this basis set, highlighting the importance of diffuse basis functions to describe the $\pi\sigma^*$ state.

In the cc-pVDZ calculation, hoppings between $\pi\pi^*$ states are the primary pathways (92% in 6-AIH^+ and 87% in 7-AIH^+). In the few remaining cases, a $\pi\sigma^*$ was populated at the time of hopping, always close to a nearly dissociated structure.

Conclusions

We investigated the excited-state dynamics of 6- and 7-AIH^+ starting from an S_3 excitation, using potential energy surface characterization and surface hopping dynamics with the ADC(2) method. Our goal was to understand why the S_3 lifetime of 6-AIH^+ is significantly shorter than that of 7-AIH^+.

Our results show that the relevant difference between the excited states of the two molecules is the geometry of the S_3 minimum. While in 6-AIH^+, it is planar, and near the Franck-Condon region, in 7-AIH^+, the 6-membered ring is puckered with a boat conformation. This boat conformation results from a pre-Dewar structure being formed between atoms C5 and C7a. This bond also occurs in 6-AIH^+ (and is even stronger there) but in the S_2 state.

The different lifetimes of the two molecules are due to the dynamic evolution between the time the molecules reach the S_3 minimum and the time they convert to the S_2 state. The $S_3 \rightarrow S_2$ hopping can happen at the entire puckering space of the 6-membered ring, and the planar minimum of 6-AIH^+ allows easy access to such conformations. In the case of 7-AIH^+, with a pre-Dewar S_3 minimum, access to $S_3 \rightarrow S_2$ hopping region depends on either increasing the puckering degree of the boat conformation or moving away to some other puckering region. Both processes take time and elongate the S_3 lifetime.

The internal conversion delay caused by the pre-Dewar minimum is also observed in the $S_2 \rightarrow S_1$ transition but to a smaller extent. In this case, 6-AIH^+ S_2 minimum has a pre-Dewar character, and the hopping to S_1 takes longer than in 7-AIH^+ with a planar S_2 minimum.

Conflicts of interest

There are no conflicts to declare.

Acknowledgements

RM, SM, MP, and MB were financially supported by the European Union's Horizon 2020 research and innovation programme ERC Advanced Grant under grant agreement no. 832237 (project SubNano). They also acknowledge the Centre de Calcul Intensif d'Aix-Marseille for granting access to its high-performance computing resources. MB and CJ acknowledge funding from the Agence Nationale de la Recherche (ANR) under the WSPLIT project (ANR-17-CE05-0005-01). The authors thank Isaure Carvin for the discussions.

References

1 J. Merour and B. Joseph, *Curr. Org. Chem.*, 2001, **5**, 471–506.
2 D. R. Motati, R. Amaradhi and T. Ganesh, *Org. Chem. Front.*, 2021, **8**, 466–513.

3 L. Merkel, M. G. Hoesl, M. Albrecht, A. Schmidt and N. Budisa, *ChemBioChem*, 2010, **11**, 305–314.
4 S.-B. Zhao and S. Wang, *Chem. Soc. Rev.*, 2010, **39**, 3142–3156.
5 L. Serrano-Andrés, M. Merchán, A. C. Borin and J. Stålring, *Int. J. Quantum Chem.*, 2001, **84**, 181–191.
6 R. Brause, M. Schmitt, D. Spangenberg and K. Kleinermanns, *Mol. Phys.*, 2004, **102**, 1615–1623.
7 M. Schmitt, C. Ratzer, K. Kleinermanns and W. Meerts, *Mol. Phys.*, 2004, **102**, 1605.
8 S. Arulmozhiraja, M. L. Coote and J.-y Hasegawa, *J. Chem. Phys.*, 2015, **143**, 204304.
9 K. Fuke and K. Kaya, *J. Phys. Chem.*, 1989, **93**, 614–621.
10 A. Douhal, S. K. Kim and A. H. Zewail, *Nature*, 1995, **378**, 260–263.
11 A. Nakajima, M. Hirano, R. Hasumi, K. Kaya, H. Watanabe, C. C. Carter, J. M. Williamson and T. A. Miller, *J. Phys. Chem. A*, 1997, **101**, 392–398.
12 J. Catalán and J. Paz, *J. Chem. Phys.*, 2005, **122**, 244320.
13 R. Crespo-Otero, N. Kungwan and M. Barbatti, *Chem. Sci.*, 2015, **6**, 5762–5767.
14 Y. N. Svartsov and M. Schmitt, *J. Chem. Phys.*, 2008, **128**, 214310.
15 D. Kina, A. Nakayama, T. Noro, T. Taketsugu and M. S. Gordon, *J. Phys. Chem. A*, 2008, **112**, 9675–9683.
16 R. Daengngern, N. Kungwan, P. Wolschann, A. J.-A. Aquino, H. Lischka and M. Barbatti, *J. Phys. Chem. A*, 2011, **115**, 14129–14136.
17 G. A. Pino, I. Alata, C. Dedonder, C. Jouvet, K. Sakota and H. Sekiya, *Phys. Chem. Chem. Phys.*, 2011, **13**, 6325–6331.
18 N. Kungwan, K. Kerdpol, R. Daengngern, S. Hannongbua and M. Barbatti, *Theor. Chem. Acc.*, 2014, **133**, 1–11.
19 H. Fang, B. K. Mai and Y. Kim, *Photochem. Photobiol.*, 2015, **91**, 306–314.
20 K. Kerdpol, R. Daengngern and N. Kungwan, *Mol. Simul.*, 2015, **41**, 1177–1186.
21 I. Lamas, R. Montero, V. Martínez-Martínez, A. Longarte and L. Blancafort, *Phys. Chem. Chem. Phys.*, 2020, **22**, 18639–18645.
22 J. Catalán, J. C. del Valle and M. Kasha, *Proc. Natl. Acad. Sci. U. S. A.*, 1999, **96**, 8338–8343.
23 O.-H. Kwon and A. H. Zewail, *Proc. Natl. Acad. Sci. U. S. A.*, 2007, **104**, 8703–8708.
24 R. Daengngern, K. Kerdpol, N. Kungwan, S. Hannongbua and M. Barbatti, *J. Photochem. Photobiol., A*, 2013, **266**, 28–36.
25 J. A. Noble, E. Marceca, C. Dedonder, W. Phasayavan, G. Féraud, B. Inceesungvorn and C. Jouvet, *Phys. Chem. Chem. Phys.*, 2020, **22**, 27280–27289.
26 R. Crespo-Otero and M. Barbatti, *Chem. Rev.*, 2018, **118**, 7026–7068.
27 G. Granucci and M. Persico, *J. Chem. Phys.*, 2007, **126**, 134114.
28 J. C. Tully, *J. Chem. Phys.*, 1990, **93**, 1061–1071.
29 T. Nelson, S. Fernandez-Alberti, A. E. Roitberg and S. Tretiak, *Acc. Chem. Res.*, 2014, **47**, 1155–1164.
30 C. Møller and M. S. Plesset, *Phys. Rev.*, 1934, **46**, 618–622.
31 T. H. Dunning Jr., *J. Chem. Phys.*, 1989, **90**, 1007–1023.
32 A. B. Trofimov, I. L. Krivdina, J. Weller and J. Schirmer, *Chem. Phys.*, 2006, **329**, 1–10.
33 A. Dreuw and M. Wormit, *Comput. Mol. Biosci.*, 2015, **5**, 82–95.
34 R. Ahlrichs, M. Bär, M. Häser, H. Horn and C. Kölmel, *Chem. Phys. Lett.*, 1989, **162**, 165–169.
35 S. G. Balasubramani, G. P. Chen, S. Coriani, M. Diedenhofen, M. S. Frank, Y. J. Franzke, F. Furche, R. Grotjahn, M. E. Harding, C. Hättig, A. Hellweg, B. Helmich-Paris, C. Holzer, U. Huniar, M. Kaupp, A. M. Khah, S. K. Khani, T. Müller, F. Mack, B. D. Nguyen, S. M. Parker, E. Perlt, D. Rappoport, K. Reiter, S. Roy, M. Rückert, G. Schmitz, M. Sierka, E. Tapavicza, D. P. Tew, C.-v Wüllen, V. K. Voora, F. Weigend, A. Wodyński and J. M. Yu, *J. Chem. Phys.*, 2020, **152**, 184107.
36 B. G. Levine, C. Ko, J. Quenneville and T. J. Martínez, *Mol. Phys.*, 2006, **104**, 1039–1051.
37 B. G. Levine, J. D. Coe and T. J. Martínez, *J. Phys. Chem. B*, 2008, **112**, 405–413.
38 M. Hillery, R. F. O'Connell, M. O. Scully and E. P. Wigner, *Phys. Rep.*, 1984, **106**, 121–167.
39 M. Barbatti and K. Sen, *Int. J. Quantum Chem.*, 2016, **116**, 762–771.
40 S. Bai, R. Mansour, L. Stojanović, J. M. Toldo and M. Barbatti, *J. Mol. Model.*, 2020, **26**, 107.
41 S. Hammes-Schiffer and J. C. Tully, *J. Chem. Phys.*, 1994, **101**, 4657–4667.
42 J. Pittner, H. Lischka and M. Barbatti, *Chem. Phys.*, 2009, **356**, 147–152.
43 M. Barbatti, M. Ruckenbauer, F. Plasser, J. Pittner, G. Granucci, M. Persico and H. Lischka, *Comput. Mol. Biosci.*, 2014, **4**, 26–33.
44 R. Mansour, S. Mukherjee, M. Pinheiro Jr and M. Barbatti, *Dataset*, 2022, DOI: **10.6084/m9.figshare.19448165.v3**.
45 M. Pinheiro Jr, S. Mukherjee and M. Barbatti, *Dataset*, 2021, DOI: **10.6084/m9.figshare.c.5478270**.
46 X. Huang, J.-P. Aranguren, J. Ehrmaier, J. A. Noble, W. Xie, A. L. Sobolewski, C. Dedonder-Lardeux, C. Jouvet and W. Domcke, *Phys. Chem. Chem. Phys.*, 2020, **22**, 12502–12514.
47 D. Cremer and J. A. Pople, *J. Am. Chem. Soc.*, 1975, **97**, 1354–1358.
48 P. Busch, in *Time in Quantum Mechanics*, ed. J. G. Muga, R. S. Mayato and I. L. Egusquiza, Springer Berlin Heidelberg, Berlin, Heidelberg, 2002, pp. 69–98, DOI: **10.1007/3-540-45846-8_3**.
49 M. Barbatti, M. Ruckenbauer and H. Lischka, *J. Chem. Phys.*, 2005, **122**, 174307.
50 M. T. do Casal, J. M. Toldo, M. Pinheiro Jr and M. Barbatti, *Open Res. Europe*, 2021, **1**, 49.